Acta Crystallographica Section D
Biological Crystallography
ISSN 0907-4449

Structure determination of tetrahydroquinazoline antifolates in complex with human and *Pneumocystis carinii* dihydrofolate reductase: correlations between enzyme selectivity and stereochemistry

Vivian Cody,[a]* Joe R. Luft,[a] Walt Pangborn,[a] Aleem Gangjee[b] and Sherry F. Queener[c]

[a]Structural Biology Department, Hauptman–Woodward Medical Research Institute, 73 High Street, Buffalo, NY 14203, USA, [b]Department of Pharmaceutical Sciences, Duquesne University, Pittsburgh, PA 15282, USA, and [c]Department of Pharmacology and Toxicology, Indiana University School of Medicine, Indianapolis, IN 46202, USA

Correspondence e-mail: cody@hwi.buffalo.edu

Received 15 December 2003
Accepted 26 January 2004

PDB References: hDHFR–(1) complex, 1s3w, r1s3wsf; pcDHFR–(1) complex, 1s3y, r1s3ysf; hDHFR–(2) complex, R3(1), 1s3u, r1s3usf; hDHFR–(2) complex, R3(2), 1s3v, r1s3vsf.

Structural data are reported for the first examples of the tetrahydroquinazoline antifolate (6*R*,6*S*)-2,4-diamino-6-(1-indolinomethyl)-5,6,7,8-tetrahydroquinazoline (1) and its trimethoxy analogue (6*R*,6*S*)-2,4-diamino-6-(3′,4′,5′-trimethoxybenzyl)-5,6,7,8-tetrahydroquinazoline (2) as inhibitor complexes with dihydrofolate reductase (DHFR) from human (hDHFR) and *Pneumocystis carinii* (pcDHFR) sources. The indoline analogue (1) was crystallized as ternary complexes with NADPH and hDHFR (1.9 Å resolution) and pcDHFR (2.3 Å resolution), while the trimethoxy quinazoline analogue (2) was crystallized as a binary complex with hDHFR in two polymorphic rhombohedral *R*3 lattices: R3(1) to 1.8 Å resolution and R3(2) to 2.0 Å resolution. Structural analysis of these potent and selective DHFR–inhibitor complexes revealed preferential binding of the 6*S*-equatorial isomer in each structure. This configuration is similar to that of the natural tetrahydrofolate substrate; that is, 6*S*. These data also show that in both the hDHFR and pcDHFR ternary complexes with (1) the indoline ring is partially disordered, with two static conformations that differ between structures. These conformers also differ from that observed for the trimethoxybenzyl ring of tetrahydroquinazoline (2). There is also a correlation between the disorder of the flexible loop 23 and the disorder of the cofactor nicotinamide ribose ring in the pcDHFR–NADPH–(1) ternary complex. Comparison of the *Toxoplasma gondii* DHFR (tgDHFR) sequence with those of other DHFRs provides insight into the role of sequence and conformation in inhibitor-binding preferences which may aid in the design of novel antifolates with specific DHFR selectivity.

1. Introduction

The enzyme dihydrofolate reductase (DHFR) catalyzes the NADPH-dependent reduction of 7,8-dihydrofolate (H_2F) to 5,6,7,8-tetrahydrofolate (H_4F; Fig. 1) and, much less efficiently, folate (FA) to H_4F. The optically active tetrahydrofolates have an asymmetric C atom at position 6 of the reduced pteridine ring in addition to their L-glutamic acid side chains (Kisliuk, 1984; Blakely, 1995). The absolute configuration of C6 in tetrahydrofolates was determined from crystallographic and biochemical studies of 5,10-methylenetetrahydrofolic acid (5,10-CH_2-H_4F; Fig. 1), which showed the absolute configuration at C6 in the reduced pyrazine ring is *R* (Fontecilla-Camps *et al.*, 1979). This corresponds to the *S* configuration in 5,6,7,8-tetrahydrofolic acid. Solution NMR data for H_4F showed that C6—H is in rapid exchange between an axial and an equatorial orientation (Poe & Hoogsteen, 1978; Poe *et al.*,

1979). These studies also showed that the preferred conformation of the tetrahydropyrazine ring is half-chair, with the C6—H axial and the benzyl ring of the *p*-aminobenzoylglutamate extended away from the pteridine ring (Poe *et al.*, 1979). Solution and structural data for 6-methyl tetrahydropterin revealed a preference for the C6-methyl to be equatorial, while in 5-formyl-6,7-dimethyltetrahydropterin the conformation is *R* at position C6 (Poe & Hoogsteen, 1978). However, when the *p*-aminobenzoylglutamate moiety was present, the preferred configuration at C6 was *S*, as observed in tetrahydrofolate. The observation that a shift in the conformational preference of C6 could be dictated by the overall structure suggested that the C6 diastereomers are of equal energy in solution and that this mechanism allows the ligands to be more widely utilized by other folate-dependent enzymes in the metabolic pathway (Poe & Hoogsteen, 1978).

6*R*,6*S*-derivatives of H_4F are also involved in a number of folate-dependent enzyme reactions. For example, 5,10-CH_2-H_4F is a substrate of thymidylate synthase (Kisliuk, 1984; Blakely, 1995), while 5,10-dideazatetrahydrofolate (ddH_4F; Fig. 1) is an inhibitor of glycinamide ribonuclease formyl transferase and is also a substrate for folylpolyglutamate synthetase (Baldwin *et al.*, 1991; Beardsley *et al.*, 1989; Moran *et al.*, 1989; Taylor *et al.*, 1992). Biological activity data for the inhibition of these enzymes would be expected to show a preferential activity for one of the diasteromers at C6. However, in the example of ddH_4F both diastereomers showed equivalent potency but against different targets in leukemia cells (Moran *et al.*, 1989; Taylor *et al.*, 1992). These data also suggested that there was little stereochemical specificity for the C6 diastereomers (Moran *et al.*, 1989). Since there is a flip in the orientation of the pterin ring of folate substrates and that of antifolates, the stereochemistry at position C6 of these inhibitors will be reversed depending on whether the compounds are folate or antifolate analogues. Also, it has been shown that the preferred diastereomer for the same folate analogue differs depending on the enzyme target (Taylor *et al.*, 1992).

Structural data for the complex of ddH_4F with *Escherichia coli* DHFR (ecDHFR; Reyes *et al.*, 1995) confirmed that the reduced pyrazine ring forms a half-chair conformation with C6 out of the plane. This puckering of the ring places C5 and C7 closer to the nicotinamide ribose-binding site than in folate. In this structure, the configuration at C6 is *R*. The largest changes on binding this diastereomer to ecDHFR, compared with folate or methotrexate (MTX) binding, is observed in the orientation of the *p*-aminobenzyl group and is a consequence of the change in hybridization of the C6 atom upon reduction of the N5—C6 bond.

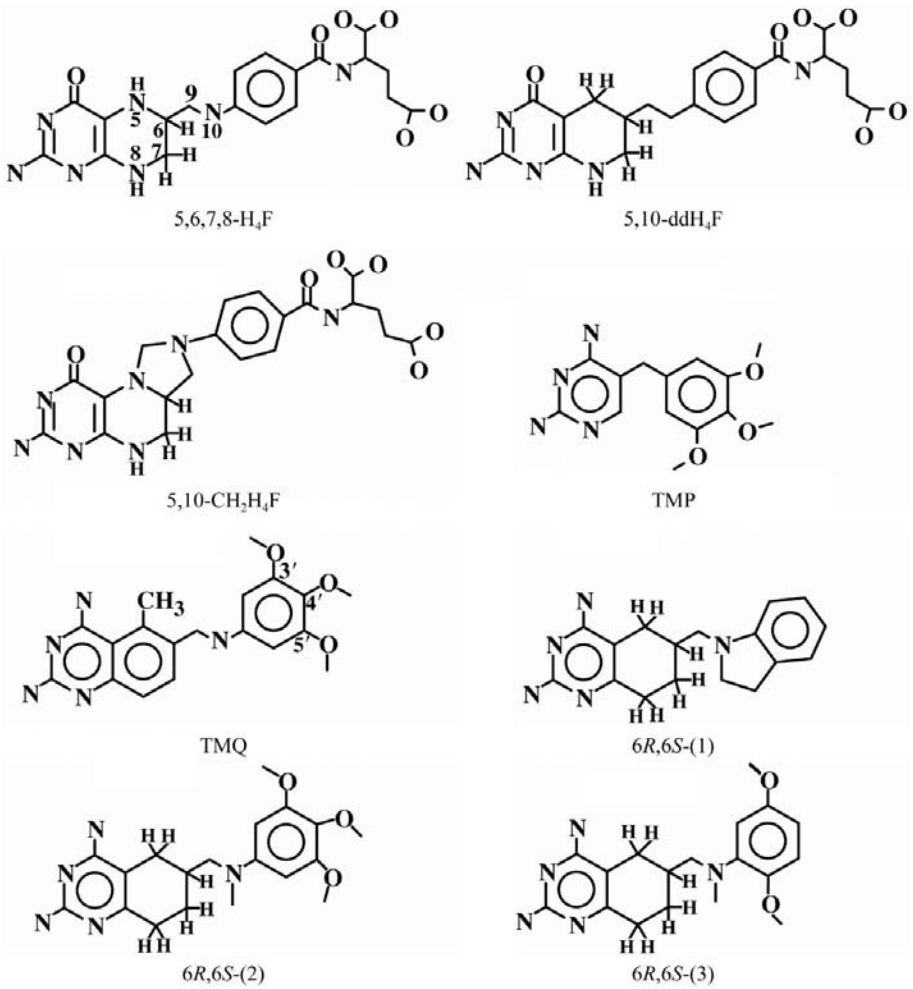

Figure 1
Schematic diagram of folate analogues.

Crystallographic data for DHFR–ligand complexes have shown that the 2-amino-4-oxo folates and 2,4-diamino antifolates differ in the orientation of their respective pterin rings, which are flipped 180° in the active site (Fig. 2). Structural data also show that the preferred stereochemistry at position C6 for these two classes of compounds is reversed (Matthews *et al.*, 1978; McCourt & Cody, 1991). Thus, the design of the appropriate isomer at C6 would depend on the specific enzyme path that was being targeted for inhibition.

Opportunistic infections with *Pneumocystis carinii* (pc) and *Toxoplasma gondii* (tg) are still among the leading causes of mortality and morbidity in patients with AIDS. Current antifolate treatments have limited efficacy and result in drug resistance (Epstein *et al.*, 1994). The antifolates trimethoprim (TMP) and trimetrexate (TMQ) (Fig. 1) are currently used in the treatment of pc and tg infections, despite their limited selectivity against these pathogens (Masur *et al.*, 1992). As part of a program to explore the design of novel antifolates with selectivity for pcDHFR

or tgDHFR, a series of 20 6-substituted 2,4-diaminotetrahydroquinazolines were synthesized as 6*R*,6*S* racemic mixtures and tested for DHFR inhibition (Gangjee *et al.*, 1995). Data from this series revealed several antifolates to be potent and to be more selective against tgDHFR than pcDHFR. For example, the most tgDHFR-selective compound was the 2′,5′-dimethoxy antifolate (3) (Fig. 1), while its trimethoxy derivative (2) was less selective (Table 1). Compound (1), on the other hand, had a similar selectivity profile, even though it has no methoxy substitutents and was conformationally restricted by cyclization about the bridging N10—C1′ bond to form the indoline ring (Fig. 1). The chiral center at the quinazoline-ring C6 position of (1) or (2) (Fig. 1) places the side chain in an axial (6*R*) or equatorial (6*S*) orientation.

Although many assays of antifolate inhibitors of DHFR have been performed using rat liver DHFR (rlDHFR) as a target, the sequence of rlDHFR was not known until recently (Wang *et al.*, 2001). These data revealed that the rlDHFR sequence is 89% homologous to the human DHFR enzyme and that the active-site residues are identical in the two sequences. However, to date structural data have not been reported for the rlDHFR enzyme. These sequence-alignment data indicate that the structural details of hDHFR can be used as a model to understand the correlation between structure and biological activity. Thus, in order to understand this pattern of potency and DHFR selectivity, the crystal structures of (1) and (2) in complex with human and/or pcDHFR were obtained.

2. Materials and methods

2.1. Crystallization and X-ray data collection

Human DHFR was isolated and purified by Blakely and coworkers as described in Chunduru *et al.* (1994) and pcDHFR was purified as described by Broughton & Queener (1991). Crystals of human DHFR with the indoline (1) or the quinazoline (2) were grown using the hanging-drop vapor-diffusion method from purified enzyme incubated with NADPH and inhibitor prior to crystallization as previously described (Cody *et al.*, 1992). Protein droplets contained 60–65% ammonium sulfate in 0.1 *M* phosphate buffer pH 6.8. Crystals of the pcDHFR complex with (1) and NADPH were grown using a thermal gradient (Luft *et al.*, 1999) in 50% PEG 2000 50 m*M* MES pH 6.0 in 100 m*M* KCl. Data were collected at room temperature on a Rigaku R-AXIS IIc area detector for the human DHFR complexes and on an R-AXIS IV for the pcDHFR complex. Although most of the pcDHFR crystals were small and of limited quality, data were collected from the best crystal that resulted in reasonable diffraction. Data for all structures were processed with *DENZO* and scaled with *SCALEPACK* (Otwinowski & Minor, 1997). The unit-cell parameters and crystal properties are listed in Table 2 for the NADPH ternary complex with inhibitor (1) with hDHFR and pcDHFR and for the two polymorphic forms of the hDHFR binary complex with inhibitor (2).

Table 1
Inhibition of selected antifolates and their IC_{50} values (n*M*) for pcDHFR, tgDHFR and rlDHFR and selectivity ratios compared with rat liver as reported by Gangjee *et al.* (1995).

Compound	pcDHFR	tgDHFR	rlDHFR	rlDHFR/ pcDHFR	rlDHFR/ tgDHFR
TMP	12000	2700	133000	1.1	49.0
TMQ	42	10	3	0.07	0.30
(1)	210	27	160	0.76	5.93
(2)	95	7	38	0.40	5.43
(3)	300	15	260	0.90	17.33

2.2. Structure determination and refinement

All structures were solved by molecular-replacement methods with *CNS* (Brünger *et al.*, 1998) using coordinates for hDHFR (PDB code 1mvs) or pcDHFR (PDB code 1d8r). Models of (1) and (2) were generated from the crystal structure of a similar analogue (Cody *et al.*, 1993) and optimized with *SYBYL* (Tripos, St Louis, MO, USA). Between least-squares minimizations, the structure was manually adjusted to fit difference electron density and verified by a series of omit maps calculated from the current model with deleted fragments. Simulated-annealing methods using the program *CNS* (Brünger *et al.*, 1998) were used to refine both hDHFR and pcDHFR complexes with inhibitor (1), while the polymorphic hDHFR–(2) binary complexes were refined with the restrained least-squares program *PROLSQ* (Hendrickson & Konnert, 1980; Finzel, 1987) in combination with the model-building program *CHAIN* (Sack, 1988). In the case of the *CNS* refinement, $R_{\rm free}$ was based on a test set with 10% selection criteria. All calculations were carried out on a Silicon Graphics Impact R10000 Workstation. All data were refined to their resolution limits (Table 2). The initial $(2|F_{\rm o}| - |F_{\rm c}|)\exp(i\alpha_{\rm c})$ maps, where $F_{\rm o}$ is the observed and $F_{\rm c}$

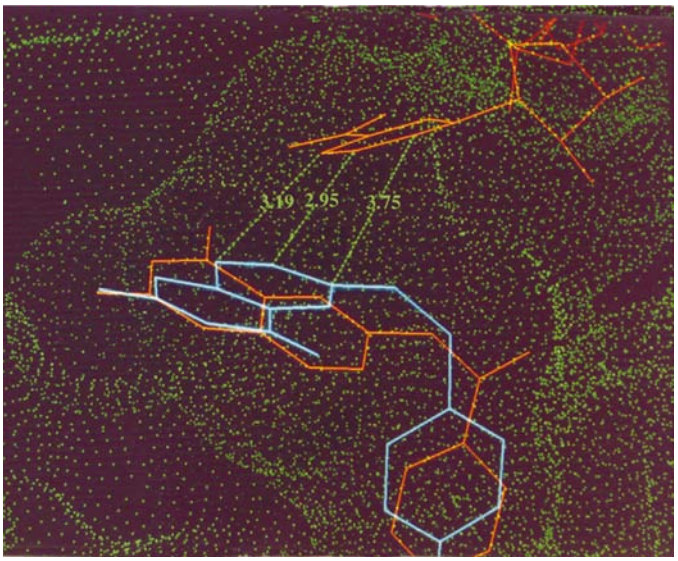

Figure 2
Orientation of the pteridine ring for folates (cyan) and antifolates (red). The Connolly surface for hDHFR is shown in green and the contact distances of the nicotinamide ring of NADPH are shown to the folate-reduction site.

Table 2
Crystal properties and refinement statistics.

Values in parentheses are for the last resolution shell.

	hDHFR–(1)	pcDHFR–(1)		hDHFR–(2), R3(1)	hDHFR–(2), R3(2)	
PDB code	1s3w	1s3y		1s3u	1s3v	
Complex	Ternary	Ternary		Binary	Binary	
Unit-cell parameters						
a (Å)	86.98	37.36		85.17	106.97	
b (Å)	86.98	43.29		85.17	106.97	
c (Å)	76.86	61.40		77.86	43.86	
γ /β (°)	120	94.65		120	120	
Space group	$R3$	$P2_1$		$R3$	$R3$	
Unit-cell volume (Å^3)	503560	95970		489118	431306	
V_M (Å^3 Da^{-1})	2.56	2.30		2.56	2.25	
Solvent content (%)	53	45		52	45	
Resolution range (Å)	50.0–1.90 (2.00–1.90)	50.0–2.25 (2.33–2.25)		50.0–2.50 (2.6–2.5)	50.0–1.80 (1.90–1.80)	
R_{merge} (%)	7.1	5.1		4.7	4.2	
Overall completeness (%)	90.1 (91.4)	73.9 (76.9)		99.1 (99.1)	90.3 (55.9)	
Total No. reflections	17079	9464		7225	15660	
No. reflections used	10995	6996		5749	13649	
R factor (%)	17.7	23.3		16.5	17.3	
R_{free} (%)	21.6	28.9		18.2	19.2	
No. protein atoms	1502	1628		1502	1502	
No. water molecules	81	18		51	111	
Ramachandran plot, residues in most favored region (%)	89.3	84.0		93.7	90.0	
B factor (protein average) (Å^2)	45.1	39.6		19.8	26.5	
Distances (Å)	R.m.s. σ†	R.m.s σ†	Target σ	R.m.s. σ‡	R.m.s. σ‡	Target σ
Bonds	0.008	0.008	0.009	0.016	0.016	0.020
Angles	1.18	1.22	1.2	0.050	0.046	0.040
B, main chain† (Å^2)	1.61	1.68	1.5			
B, side chain† (Å^2)	2.25	1.88	2.0			
B, bond angle†	2.74	2.93	2.0			
B, side-chain angle† (Å^2)	3.5	2.81	2.5			
Planar 1–4				0.051	0.048	0.050
Planar groups				0.012	0.015	0.020
Chiral volume				0.163	0.174	0.150
Single torsion				0.219	0.190	0.500
Multiple torsion				0.271	0.235	0.500
Possible hydrogen bonds				0.219	0.216	0.500
Torsion angles (°)						
Planar				2.2	3.2	3.0
Staggered				22.9	19.9	15.0
Orthonormal				21.6	17.9	20.0

† Values from *CNS* refinement. ‡ Values from *PROLSQ* refinement.

the calculated structure factor based on the protein model only and α_c is the calculated phase, resulted in electron density corresponding to the inhibitor and cofactor for the complexes with (1), but not for the cofactor in both the hDHFR–(2) structures. Two sulfate groups from the precipitating agent occupy the pyrophosphate positions of NADPH and water molecules fill the nicotinamide-ring pocket in these binary structures. The Ramachandran conformational parameters generated by *PROCHECK* (Laskowski *et al.*, 1993) for the final models from the last cycle of refinement show that for the hDHFR and pcDHFR complexes with (1) between 84 and 90%, respectively, of the residues have the most favored conformation and none are in disallowed regions. For both polymorphic hDHFR binary complexes with (2) these values are between 90 and 94%, respectively (Table 2). Coordinates for these structures have been deposited with the PDB (Table 2).

Despite the relatively poor quality and resolution of the data for the pcDHFR inhibitor complex with (1), the results are consistent with those from the structure of the hDHFR inhibitor complex with (1). The difference electron-density maps for both the hDHFR and pcDHFR complexes (Figs. 3 and 4) show that in the complexes with (1) the indoline ring was partially disordered, with major populations in two static positions (Fig. 3). In the case of the hDHFR complex, the orientation with the larger occupancy (75%) placed the indoline ring in a pocket near Leu22 and the nicotinamide ribose ring and the lower population indoline ring was placed in the *p*-aminobenzoylglutamate pocket, as observed for most other inhibitors. The disorder in the hDHFR complex also results in partial occupancy of the Phe31 phenyl ring in order to accommodate this movement. However, in the case of the pcDHFR–NADPH–(1) complex, in addition to the disorder in the position of the indoline ring, which differs from that observed in the hDHFR complex, there is also disorder in the occupancy of the nicotinamide-ribose ring that indicates that this portion of NADPH is highly mobile as shown by the lack of clearly identifiable electron density in this region (Fig. 3*b*); this moiety is likely to have moved toward the surface of the enzyme. Similar disorder of the nicotinamide portion of the cofactor has also been observed in the ecDHFR complex with folate (Bystroff *et al.*, 1990). The lower quality of the pcDHFR complex data also contributed to the difficulty in modeling the flexible regions near loops 23 and 47 (Fig. 5).

There is a clear indication of binary complex formation in the case of the two polymorphic hDHFR complexes with (2) (Fig. 4). The electron density shows the presence of sulfate ions from the buffer at the phosphate positions of NADPH, as observed in other binary complexes (Cody *et al.*, 1993, 2003).

3. Results

The overall characteristics of the fold in these hDHFR and pcDHFR complexes are similar to those reported previously (Chunduru *et al.*, 1994; Cody *et al.*, 1992, 1993, 1999, 2003; Cody, Galitsky, Luft, Pangborn *et al.*, 2002; Cody, Galitsky,

Luft, Rosowsky *et al.*, 2002; Gangjee *et al.*, 1998) (Fig. 5). In the pcDHFR ternary complex with (1) and NADPH, there are conformational differences in the flexible-loop regions encompassing loops 23 (residues 19–25), 47 (residues 42–49) and 100 (residues 88–103) compared with other pcDHFR complexes (Cody *et al.*, 1999; Cody, Galitsky, Luft, Pangborn *et al.*, 2002; Cody, Galitsky, Luft, Rosowsky *et al.*, 2002). The lack of interpretable electron density for loops 23 and 47 of this pcDHFR complex indicates that these regions are highly mobile and that the conformation observed represents an alternate conformational state compared with those observed in other pcDHFR complexes (Cody *et al.*, 1999; Cody, Galitsky, Luft, Pangborn *et al.*, 2002; Cody, Galitsky, Luft, Rosowsky *et al.*, 2002).

Structural analyses of several ecDHFR–ligand complexes have shown that the Met20 loop, which corresponds to loop 23 in the pcDHFR structures, is highly mobile, reflecting ligand-induced conformational changes that occur on binding the cofactor (Sawaya & Kraut, 1997). Similar data for pcDHFR revealed that loop 23 was observed in a 'flap-open' or 'flap-closed' position over the nicotinamide ribose ring of the cofactor involved in ligand binding (Cody *et al.*, 1999). In the pcDHFR–NADPH–(1) ternary complex, there was density showing bound cofactor; however, the poor electron density for the nicotinamide ribose ring showed it was disordered, with no obvious alternative position for the nicotinamide ribose ring observed. Similar disorder of the cofactor was observed in the ecDHFR complex with $NADP^+$ and folate (Bystroff *et al.*, 1990), as well from solution NMR data for a thionicotinamide cofactor analogue bound to *Lactobacillus casei* DHFR, in which it was proposed that the nicotinamide ribose ring was positioned towards the enzyme surface (Feeney *et al.*, 1983). The lack of interpretable electron density for the nicotinamide ribose ring of NADPH and the poor electron density for loop 23 in this pcDHFR–NADPH–(1) complex are consistent with the conformational mobility of this interaction.

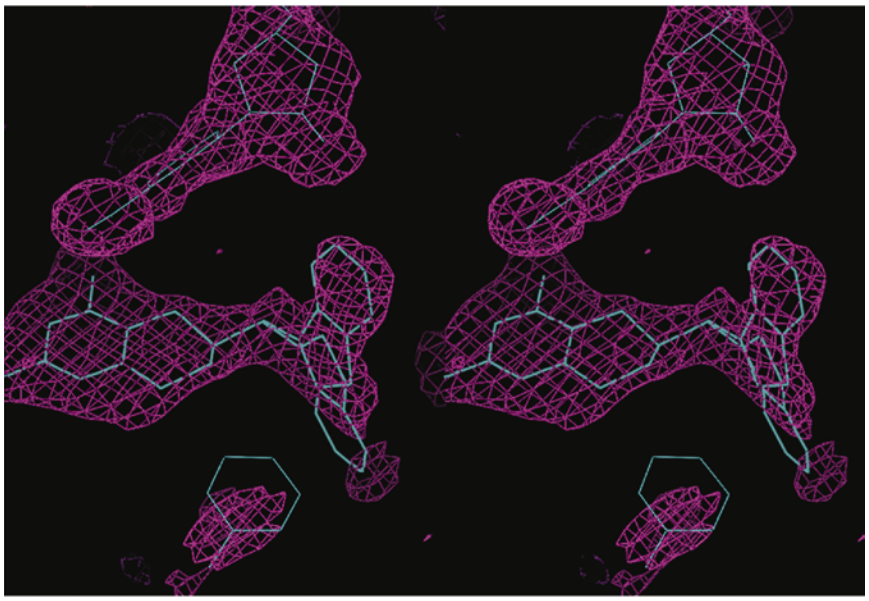

(*a*)

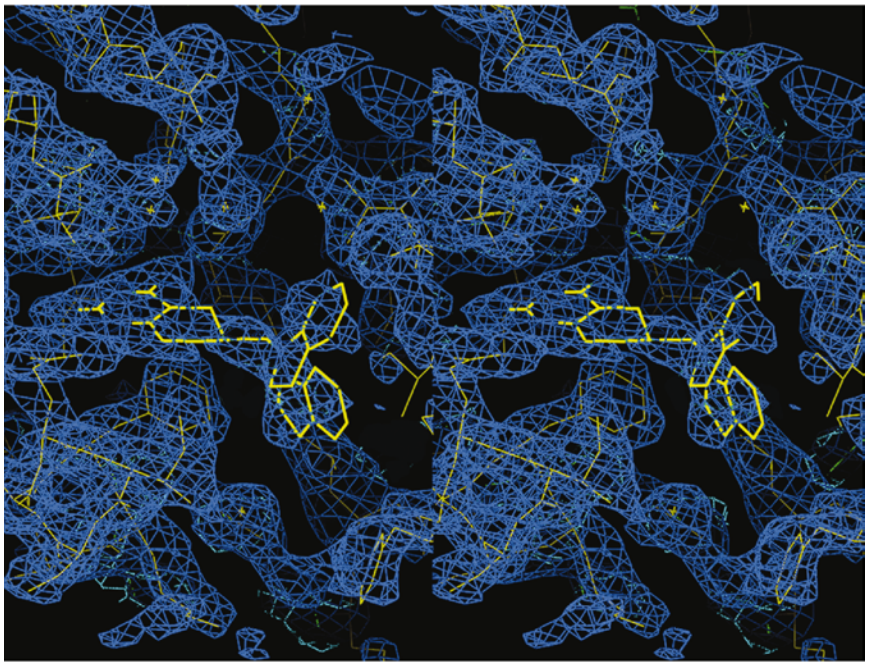

(*b*)

Figure 3
(*a*) Difference ($F_o - F_c$, 1σ) electron density for hDHFR binary complex with (1) calculated as an inhibitor cofactor omit map from the last cycle of refinement, highlighting the NADPH and Phe31 positions. (*b*). Difference ($2F_o - F_c$, 1σ) electron density for pcDHFR complex with (1). Note the absence of the nicotinamide ribose ring in the electron density.

Differences in the packing interactions between the two polymorphic *R*3 lattices result in small changes in the surface-loop conformations between the two hDHFR–(2) binary complexes. These differences are smaller than observed for other *R*3 polymorphic hDHFR binary complexes (Cody *et al.*, 2003). The major changes involve differences (0.5–1.0 Å) in the loop regions 20 (residues 16–25), 44 (residues 40–48), 84 (residues 81–89), 103 (residues 99–108), 146 (residues 143–148) and 164 (residues 161–169).

3.1. Inhibitor binding

The interactions of the 2,4-diamino quinazoline ring of inhibitors (1) and (2) preserve the overall pattern of contacts with invariant residues in the hDHFR and pcDHFR active sites. As observed in other DHFR–inhibitor complexes, a hydrogen-bond network involving structural water, the conserved residues Thr136, Glu30 and Trp24

(hDHFR numbering) and the N1 nitrogen and 2-amino group of inhibitors (1) and (2) is maintained. Since the N atoms at positions 5 and 8 of the inhibitors have been replaced by carbon, the hydrogen-bond network involving N8 and the enzyme is disrupted. Similarly, the inhibitor 4-amino group maintains its contacts with the conserved residues Ile7 and Tyr121.

The tetrahydroquinazolines antifolates were synthesized as (6*R*,6*S*) racemic mixtures so that either or both enantiomorphs could be represented in the binding site. The interpretation of these structural data reveal that inhibitors (1) and (2) bind to both hDHFR and pcDHFR in an equatorial 6*S* conformation with the tetrahydroquinazoline ring in a twist-chair or half-chair conformation (Table 3). There is no electron-density evidence to indicate the presence of the 6*R*-axial isomer. As illustrated (Fig. 6), the model for the axial 6*R* conformation of (1) makes several unfavorable contacts within the binding site. Energy minimization of the 6*R* and 6*S* isomers of (1) carried out by Gangjee *et al.* (1995) indicated the 6*R* (axial) isomer to be 4 kJ mol^{-1} higher in energy than the 6*S* (equatorial) isomer. These modeling data also indicated that these conformers did not superimpose on that of TMQ when bound in the hDHFR crystal structure (Cody *et al.*, 1993; Fig. 7).

Table 3
Tetrahydroquinazoline and pteridine inhibitor conformations.

Torsion	hDHFR –(1)	pcDHFR –(1)	hDHFR –(2), R3(1)	hDHFR –(2), R3(2)	ecDHFR –ddH$_4$F
C4—C4a—C5—C6	−158	−155	175	164	154
C4a—C5—C6—C7	−49	−54	−12	47	41
C5—C6—C7—C8	59	55	−7	−54	−51
C6—C7—C8—C8a	9	−28	12	−11	32
C4a—C5—C6—C9	−172	−179	179	172	−81
C5—C6—C9—N10	151	−126	140	172	−66

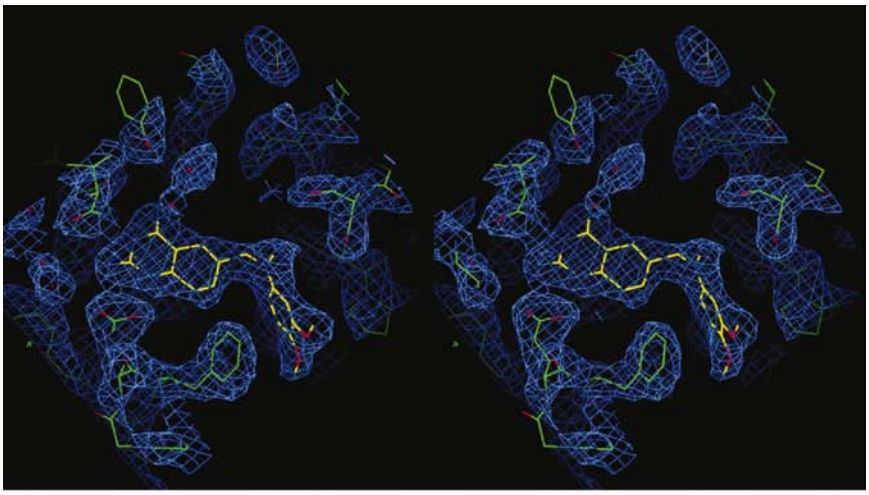

(*a*)

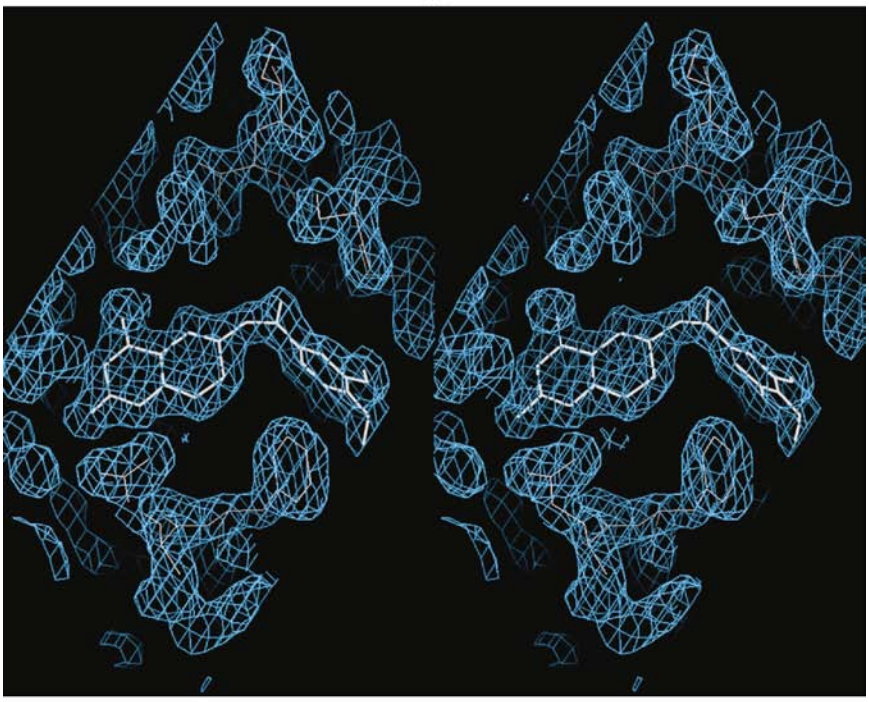

(*b*)

Figure 4
(*a*) Difference ($2F_o - F_c$, 1σ) electron density for hDHFR complex with (2) for polymorph R3(1). (*b*) Difference ($2F_o - F_c$, 1σ) electron density for hDHFR complex with (2) for polymorph R3(2).

The tetrahydroquinazoline ring of inhibitor (1) has a twist-chair conformation with the positions of C6 and C7 reversed from those observed in the hDHFR binary complexes with (2). In the case of the R3(1) lattice, inhibitor (2) has a more flattened half-chair, while the conformation of (2) in the R3(2) lattice is a twist-chair with C6 up and C7 down relative to the planar pteridine ring of folate or MTX (Cody *et al.*, 1999). These conformations are similar to that observed for the ecDHFR–ddH$_4$F complex (Reyes *et al.*, 1995), in which C6 is puckered down away from the nicotinamide-binding pocket. However, it should be noted that the binding of the pteridine ring is flipped relative to the binding of the diaminopterine antifolates (Matthews *et al.*, 1978; McCourt & Cody, 1991). Thus, the configuration at C6 is the opposite racemate observed for ddH$_4$F.

In the case of the hDHFR–NADPH–(1) complex, the indoline ring of (1) is present in two orientations with 75% occupancy for the indoline ring positioned toward residue Leu22 and 25% toward Ile60 (Fig. 8). As a consequence of the partial occupancy of the indoline ring bound in the *p*-aminobenzoylglutamate pocket, the side chain of Phe31 adopts an alternate conformation compared with that observed in other hDHFR–inhibitor complexes (Cody *et al.*, 1993). Similarly, the pcDHFR complex with (1) also shows the indoline ring of (1)

present in two orientations, with 80% occupancy for the indoline ring toward Ile65 and 20% occupancy for the conformer toward Leu25. In this structure, the 6*S* conformer is preferentially bound in the active site, although with a different conformation than found in the hDHFR complex (Table 3; Fig. 8).

The orientations of the indoline ring in both the hDHFR and pcDHFR complexes also differ from that observed for the trimethoxybenzyl ring of TMQ (Cody *et al.*, 1993) and that observed for the tetrahydroquinazoline 2 (Fig. 7). In the binary hDHFR complexes with (2) and TMQ, the 3′-methoxy group makes intermolecular contacts with residues Phe31 and Pro61 in the active site. In the R3(2) polymorph, there are also close contacts to Leu22 and Asp21 that are longer (>3.5 Å) in the other structures. A structural water molecule is also positioned within hydrogen-bonding contact of both the 3′-O and 4′-O atoms. The 4′-O and 5′-O atoms make close contact to the functional groups of Asn64 in these binary complexes, while the 4′- and 5′-methoxy C atoms make hydrophobic contacts with Leu67 and, depending on their conformations, Phe31 and Phe34.

The observation of two polymorphic *R*3 lattices for the binary complex of hDHFR with (2) provides an opportunity to compare the influence of packing interactions on the conformations of surface loops in these structures. Comparison of the two polymorphic lattices for the hDHFR–(2) complex reveals that the *R*3(2) lattice is more compact, as indicated by the smaller V_M value and smaller solvent content (Table 2) than the *R*3(1) lattice. These results are similar to the polymorphic *R*3 lattices reported for other binary hDHFR–inhibitor complexes (Cody *et al.*, 2003). The packing of the hDHFR–(2) *R*3(1) lattice is also more compact than that observed for the ternary complex hDHFR–NADPH–(1). A key feature of the packing in the *R*3(1) lattice is that the enzyme is oriented such that Lys63 forms symmetrical Nz···Nz hydrogen bonds about the threefold axis that relate the Lys63 residues. The tightness of the packing of the enzyme about the threefold axis is a function of the Lys63 side-chain conformation. In these hDHFR complexes with an *R*3(1)

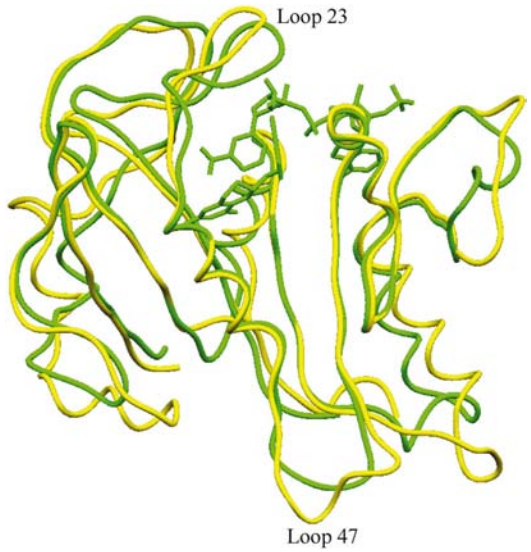

Figure 5
Superposition of the tertiary structures of pcDHFR (yellow) with hDHFR (green) bound with inhibitor (1) and NADPH. The flexible loops at 23 and 47 are highlighted. Figure produced with *SETOR* (Evans, 1993).

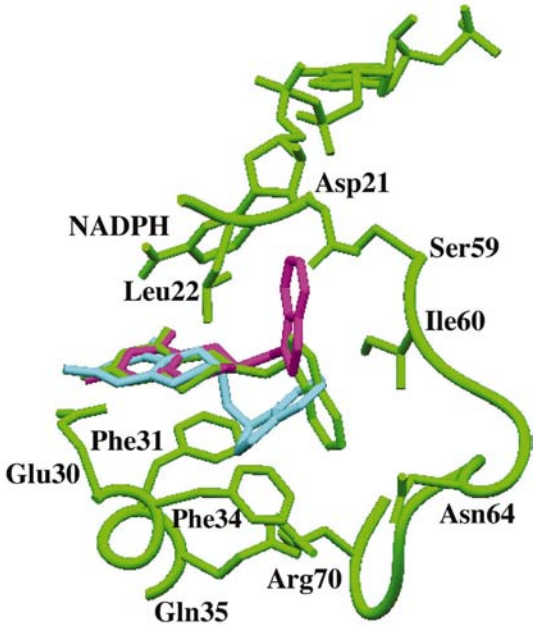

Figure 6
Comparison of the binding of the equatorial isomer of (1) observed in two partially disordered positions (violet and green) for hDHFR (green) and with the axial isomer (cyan) modeled into the active site. Active-site residues are highlighted (hDHFR numbering). Diagram produced with *SETOR* (Evans, 1993).

Figure 7
Comparison of the binding interactions of (1) (green, pcDHFR; yellow, hDHFR), (2) (red, hDHFR) and TMQ (magenta, hDHFR). Highlighted are the side chains at positions (hDHFR numbering) Glu30, Phe31, Lys35, Leu22 and Asn64 and NADPH as labeled in the previous figure. Figure produced with *SETOR* (Evans, 1993).

lattice, the contact of Lys63 Nz is 8.2 Å for the binary complex with (2) and 10.9 Å for the ternary complex with (1). These values are larger than reported previously (4.3 Å; Cody *et al.*, 2003), but within the range observed for MTX (8.5 Å; Cody *et al.*, 1993).

4. Discussion

This is the first report of the structures of tetrahydroquinazoline antifolates bound to either human or *P. carinii* DHFR. Although these antifolates were synthesized and tested as 6*R*,6*S* racemic mixtures (Gangjee *et al.*, 1995), structural data show that both tetrahydroquinazolines (1) and (2) bind the 6*S*-equatorial enantiomorph. These data further reveal conformational flexibility in the binding mode for the tetrahydroquinazoline (1). The indoline ring of (1) is observed in two partially occupied static conformations that probe different parts of the DHFR active site in both the hDHFR and pcDHFR complexes.

Previous studies (Gangjee *et al.*, 1995) showed that the 6*R* racemate of these tetrahydroquinazoline antifolates has a higher energy than the 6*S* racemate and binding models of the 6*R*-(1) in hDHFR show that it makes unfavorable intermolecular contacts within the DHFR active site. Although the four conformational models for the indoline ring of (1) probe different regions of the DHFR active site, none fully fills the space that would be occupied by the 6*R* racemate (Fig. 6).

The structure–activity correlations illustrated in Table 1 suggest that the natural flexibility of the geometry of the indoline group is a contributing factor to the enhanced selectivity of (1) compared with that of the trimethoxy quinazoline (2) or its parent antifolate TMQ. These data suggest that there is compensation between interactions involving the methoxy substituents of (2) and TMQ and those of the indoline ring. The observation of multiple static orientations for the indoline ring indicates that it can enhance its favorable interactions by probing new regions of the active site. The space occupied by the conformer of (1) that binds toward the cofactor position is similar to that probed by the dibenzazepine ring of the pcDHFR–NADPH ternary complex with *N*-(2,4-diaminopteridin-6-yl)methyldibenz[*b*,*f*]azepine, which is also highly selective for pcDHFR (Cody, Galitsky, Luft, Rosowsky *et al.*, 2002). Thus, these inhibitors are the first to show that binding to this region of the DHFR active site results in increased potency or selectivity.

In the case of tetrahydroquinazoline (2), there is a sixfold enhancement in its selectivity for pcDHFR compared with TMQ, a trimethoxy antifolate with a saturated quinazoline ring and a 5-methyl substitution (Fig. 1). As highlighted in Fig. 7, the overall conformation of TMQ and (2) are similar, with the major differences involving the deviation from planarity of the quinazoline ring by the saturated *B* ring of (2) and by the absence of the 5-methyl interactions observed in TMQ. The N10-methyl of (2), which is absent in TMQ, is directed toward Leu25 of the pcDHFR structure.

The presence of only two methoxy substituents in the 2′ and 5′ positions of (3), compared with the 3,4,5-substitution pattern of TMQ and (2), suggest that there are preferential contacts of the 2′-methoxy group with the active-site residues. Removal of the 3′-methoxy group in (3) would reduce the unfavorable contacts with Asp21 of the hDHFR, which in the case of pcDHFR is Ser. However, the loss of the 4′-methoxy in (3) would also cause the loss of the favorable interactions with Asn64 in hDHFR, which is replaced by Phe in pcDHFR.

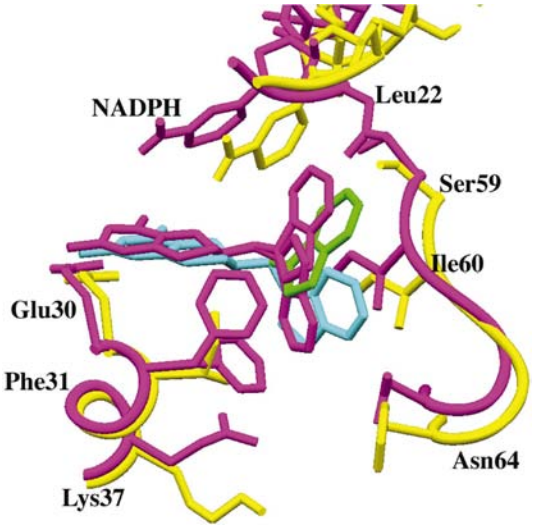

Figure 8
Comparison of the binding of inhibitor (1) to human DHFR (violet) and pcDHFR (yellow). In each structure the indoline ring of (1) is disordered. There are two orientations observed in the human DHFR structure (violet) and two orientations observed in the pcDHFR complex (green and cyan). Diagram produced with *SETOR* (Evans, 1993).

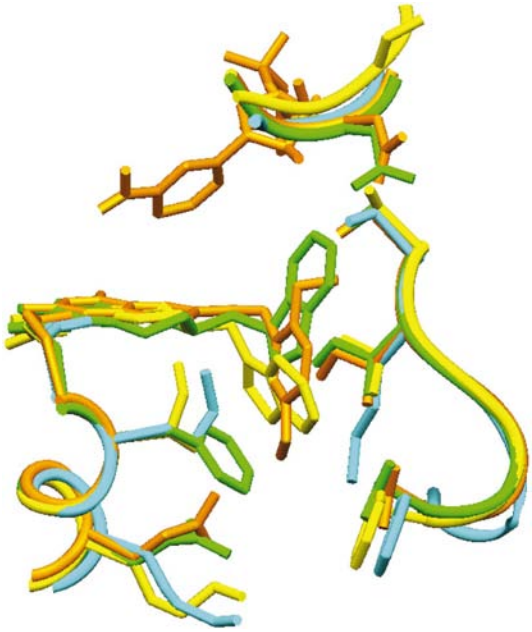

Figure 9
Composite model of tgDHFR binding interactions with (1) (yellow, pcDHFR; green, hDHFR) and the quinazoline derivative of (3) (gold, hDHFR). The side chains at position (hDHFR numbering) Glu30, Phe31, Lys35, Ile60 and Asn64 are shown as labeled in Fig. 8. Those positions in the tgDHFR sequence (cyan) that differ from hDHFR or pcDHFR are shown. Diagram produced with *SETOR* (Evans, 1993).

In order to understand the tgDHFR selectivity profile for these antifolates, the active site of tgDHFR was modeled (Cody, 2002) by comparing the sequence alignments of DHFR from several species for which crystallographic data are available (*i.e.* human, *P. carinii*, *M. tuberculosis* and *Leishmania major*; Reyes *et al.*, 1995; Cody *et al.*, 1999; Cody, Galitsky, Luft, Pangborn *et al.*, 2002; Li *et al.*, 2000; Knighton *et al.*, 1994). Although tgDHFR is significantly larger than either human or pcDHFR (250 residues compared with 186 and 207, respectively), key active-site residues are conserved (Roos, 1993; Cody, 2002; Klon *et al.*, 2002). The major differences between the active-site residues of human/pc/tgDHFR, respectively, are at positions (human numbering) 21 (Asp/Ser/Gly), 30 (Glu/Ile/Asp), 31 (Phe/Ile/Phe), 35 (Gln/Lys/Ser), 60 (Leu/Ile/Met) and 64 (Asn/Phe/Phe).

The greater selectivity of the dimethoxy compound (3) (Fig. 1; Table 1) for tgDHFR may reflect preferential contacts of the 2′-methoxy group with the active-site residues, compared with those of the 3′,4′,5′-trimethoxy substituents. As previously shown, removal of the 3′-methoxy group in compound (3) would reduce the unfavorable contacts with Asp21 of hDHFR, which is Gly in tgDHFR. In the case of tgDHFR, there is a further substitution of Ile60 by Met that may enhanced interactions with the 5′-methoxy group of antifolate (3) (Fig. 9). Therefore, the methoxybenzyl ring-substitution pattern that interacts with the most highly variable sequences among these DHFR enzymes will have the greatest potential to impact on potency and selectivity. These residue changes provide differences in specific active-site interactions among these DHFR enzymes that may influence antifolate selectivity. For example, differences in the acidic residue 30 affect the precise positioning of the diaminoquinazoline ring, while changes in the other residues, particularly at positions 60 and 64, involve interactions with the hydrophobic side chain of antifolates (1), (2) and (3) (Fig. 1).

Finally, it should be reiterated that the configuration at C6 of tetrahydroquinazoline or tetrahydropteridines will be of the opposite racemate when present in 2-oxo-4-amino folates or 2,4-diamino antifolates. In some cases the racemic mixture may prove to be more efficacious, as the optimal binding configuration can depend upon which enzyme in the folate-dependent pathway is being targeted. To validate the selection of the C6-*S* racemate as the more active antifolate in this study, these compounds should be resynthesized and tested as pure racemates.

This work was supported in part from NIH grants GM51670 (VC), GM40998 (AG) and NIH contract NO1-AI-35171 (SFQ).

References

Baldwin, S. W., Tse, A., Gossett, L. S., Taylor, E. C., Rosowsky, A., Shih, C. & Moran, R. G. (1991). *Biochemistry*, **30**, 1997–2006.

Beardsley, G. P., Moroson, B. A., Taylor, E. C. & Moran, R. G. (1989). *J. Biol. Chem.* **264**, 328–333.

Blakely, R. L. (1995). *Adv. Enzymol. Rel. Areas Mol. Biol.* **70**, 23–102.

Broughton, M. C. & Queener, S. F. (1991). *Antimicrob. Agents Chemother.* **35**, 1348–1355,

Brünger, A. T., Adams, P. D., Clore, G. M., DeLano, W. L., Gros, P., Grosse-Kunstleve, R. W., Jiang, J.-S., Kuszewski, J., Nilges, M., Pannu, N. S., Read, R. J., Rice, L. M., Simonson, T. & Warren, G. L. (1998). *Acta Cryst.* D**54**, 905–921.

Bystroff, C., Oately, S. J. & Kraut, J. (1990). *Biochemistry*, **29**, 3263–3277.

Chunduru, S. K., Cody, V., Luft, J. R., Pangborn, W., Appleman, J. R. & Blakley, R. L. (1994). *J. Biol. Chem.* **269**, 9547–9555.

Cody, V. (2002). *Chemistry and Biology of Pteridines and Folates*, edited by S. Milstien, G. Kapatos, R. A. Levine & B. Shane, pp. 525–529. Boston: Kluwer Academic Publishers.

Cody, V., Galitsky, N., Luft, J. R., Pangborn, W. & Gangjee, A. (2003). *Acta Cryst.* D**59**, 654–661.

Cody, V., Galitsky, N., Luft, J. R., Pangborn, W., Queener, S. F. & Gangjee, A. (2002). *Acta Cryst.* D**58**, 1393–1399.

Cody, V., Galitsky, N., Luft, J. R., Rosowsky, A. & Queener, S. F. (2002). *Acta Cryst.* D**58**, 946–954.

Cody, V., Galitsky, N., Rak, D., Luft, J. R., Pangborn, W. & Queener, S. F. (1999). *Biochemistry*, **38**, 4303–4312.

Cody, V., Luft, J. R., Ciszak, E., Kalman, T. I. & Freisheim, J. H. (1992). *Anticancer Drug Des.* **7**, 483–491.

Cody, V., Wojtczak, A., Kalman, T. I., Freisheim, J. H. & Blakley, R. L. (1993). *Adv. Exp. Med. Biol.* **338**, 481–486.

Epstein, L. J., Meyer, R. D, Antonson, S., Strigle, M. & Mohsenifar, Z. (1994). *Am. J. Respir. Crit. Care Med.* **150**, 1456–1459.

Evans, S. V. (1993). *J. Mol. Graph.* **11**, 134–138.

Feeney, J., Birdsall, B., Roberts, G. C. K. & Burgen, A. S. V. (1983). *Biochemistry*, **22**, 628–633.

Finzel, B. C. (1987). *J. Appl. Cryst.* **20**, 53–55.

Fontecilla-Camps, J. C., Bugg, C. E., Temple, C. Jr, Rose, J. D., Montgomery, J. A. & Kisliuk, R. L. (1979). *J. Am. Chem. Soc.* **101**, 6114–6115.

Gangjee, A., Guo, X., Queener, S. F., Cody, V., Galitsky, N., Luft, J. R. & Pangborn, W. (1998). *J. Med. Chem.* **41**, 1263–1271.

Gangjee, A., Zaveri, N., Kothare, M. & Queener, S. F. (1995). *J. Med. Chem.* **38**, 3660–3666.

Hendrickson, W. A. & Konnert, J. H. (1980). *Computing in Crystallography*, edited by R. Diamond, S. Ramaseshan & K. Venkatesan, pp. 13.01. Bangalore: Indian Academy of Sciences.

Kisliuk, R. L. (1984). *Folate Antagonists As Therapeutic Agents*, edited by F. M. Sirotnak, J. J. Burchall, W. D. Ensminger & J. A. Montgomery, Vol. 1, pp 1–69. New York: Academic Press.

Klon, A. E., Heroux, A., Ross, L. J., Pathak, V., Johnson, C. A., Piper, J. R. & Borhani, D. W. (2002). *J. Mol. Biol.* **320**, 677–693.

Knighton, D. R., Kan, C.-C., Howland, E., Janson, C. A., Hostomska, Z., Welsh, K. M. & Matthews, D. A. (1994). *Nature Struct. Biol.* **1**, 186–194.

Laskowski, R. A., MacArthur, M. W., Moss, D. S. & Thornton, J. M. (1993). *J. Appl. Cryst.* **26**, 283–291.

Li, R., Sirawaraporn, R., Chitnumsub, P., Sirawaraporn, W., Wooden, J., Athappilly, F., Turley, S. & Hol, W. G. J. (2000). *J. Mol. Biol.* **295**, 307–323.

Luft, J. R., Rak, D. M. & DeTitta, G. T. (1999). *J. Cryst. Growth*, **196**, 447–455.

McCourt, M. & Cody, V. (1991). *J. Am. Chem. Soc.* **113**, 6634–6639.

Masur, H., Polis, M. A., Tuazon, C. U., Ogata-Arakaki, D., Kovacs, J. A., Katz, D., Hilt, D., Simmons, T., Feuerstein, I., Lundren, B., Lane, H. C., Chabner, B. A. & Allegra, C. J. (1992). *J. Infect. Dis.* **167**, 1422–1426.

Matthews, D. A., Alden, R. A., Bolin, J. T., Filman, D. J., Freer, S. T., Hamlin, R., Hol, W. G. J., Kisliuk, R. L., Pastore, J., Plante, L. T., Xuong, N. H. & Kraut, J. (1978). *J. Biol. Chem.* **253**, 6946–6954.

Moran, R. G., Baldwin, S. W., Taylor, E. C. & Shih, C. (1989). *J. Biol. Chem.* **264**, 21047–21051.

Otwinowski, Z. & Minor, W. (1997). *Methods Enzymol.* **276**, 307–326.

Poe, M. & Hoogsteen, K. (1978). *J. Biol. Chem.* **253**, 543–546.

Poe, M., Jackman, L. M. & Benkovic, S. J. (1979). *Biochemistry*, **18**, 5527–5530.
Reyes, V. M., Sawaya, M., Brown, K. A. & Kraut, J. (1995). *Biochemistry*, **34**, 2710–2723.
Roos, D. S. (1993). *J. Biol. Chem.* **268**, 6269–6280.
Sack, J. S. (1988). *J. Mol. Graph.* **6**, 224–225.
Sawaya, M. R. & Kraut, J. (1997). *Biochemistry*, **36**, 586–603.
Taylor, E. C., Kuhnt, D., Shih, C., Rinzel, S. M., Grindey, G. B., Barredo, J., Jannatipour, M. & Moran, R. G. (1992). *J. Med. Chem.* **35**, 4450–4454,
Wang, Y., Bruenn, J. A., Queener, S. F. & Cody, V. (2001). *Antimicrob. Agents Chemother.* **45**, 2517–2523.